


# Iron(III)–Quercetin Complex: In Vivo Acute Toxicity and Biodistribution of Novel MRI Agent

Phattarawadee Innuan<sup>1,2</sup>, Sarawut Kongkarnka<sup>3</sup>, Atigan Thongtharb<sup>4</sup>, Jiraporn Kantapan<sup>1,2</sup>, Nathupakorn Dechsupa<sup>1,2</sup> 

<sup>1</sup>Molecular Imaging and Therapy Research Unit, Department of Radiologic Technology, Faculty of Associated Medical Sciences, Chiang Mai University, Chiang Mai, 50200, Thailand; <sup>2</sup>Department of Radiologic Technology, Faculty of Associated Medical Sciences, Chiang Mai University, Chiang Mai, 50200, Thailand; <sup>3</sup>Department of Pathology, Faculty of Medicine, Chiang Mai University, Chiang Mai, 50200, Thailand; <sup>4</sup>Department of Companion Animal and Wildlife Clinic, Faculty of Veterinary Medicine, Chiang Mai University, Chiang Mai, 50100, Thailand

Correspondence: Nathupakorn Dechsupa; Jiraporn Kantapan, Molecular Imaging and Therapy Research Unit, Department of Radiologic Technology, Faculty of Associated Medical Sciences, Chiang Mai University, Chiang Mai, 50200, Thailand, Email nathupakorn.d@cmu.ac.th; Jiraporn.kan@cmu.ac.th

**Background:** The iron(III)–quercetin complex, known as “IronQ”, is an innovative MRI contrast agent composed of one Fe(III) ion and two quercetin molecules. IronQ is efficiently internalized by cells, enabling T1-weighted MRI tracking. It has demonstrated therapeutic benefits in reducing inflammation in an intracerebral hemorrhage (ICH) mouse model and offers a safer alternative to gadolinium-based agents by avoiding cytotoxicity and genotoxicity. These properties make IronQ a promising candidate for safe and effective MRI contrast enhancement.

**Purpose:** This study aims to further the development of IronQ as an MRI contrast agent by investigating its biodistribution, pharmacokinetics, and acute toxicity in a preclinical animal model.

**Methods:** The relaxivity of IronQ was measured in water and whole blood phantoms. Acute toxicity was evaluated in Sprague Dawley rats administered single intraperitoneal doses of IronQ (75, 150, and 225  $\mu\text{mol Fe/kg BW}$ ) over a 14-day period. Pharmacokinetic studies were performed at a dose of 150  $\mu\text{mol Fe/kg BW}$ , with blood iron content analyzed using ICP-OES. For in vivo biodistribution, SD rats were administered an intravenous dose of IronQ (225  $\mu\text{mol Fe/kg BW}$ ), followed by MR imaging using a 1.5 T scanner and subsequent tissue-ICP analysis.

**Results:** The longitudinal relaxivity ( $r_1$ ) of IronQ was measured to be 2.17  $\text{mm}^{-1}\text{s}^{-1}$  in ultrapure water and 3.56  $\text{mm}^{-1}\text{s}^{-1}$  in whole blood. Acute toxicity studies showed no mortality, morbidity, or significant biochemical changes, with histopathology confirming no irreversible organ damage. Pharmacokinetics revealed peak blood iron content at 1.1 hours post-administration and clearance within 24 hours. MRI demonstrated enhanced T1 signal intensity, particularly in the liver and kidney.

**Conclusion:** These findings provide valuable insights into the safety, pharmacokinetics, and imaging efficacy of IronQ, highlighting its potential as a robust and biocompatible MRI contrast agent.

**Keywords:** magnetic resonance imaging, contrast agent, in vivo toxicity, biodistribution, IronQ

## Introduction

Magnetic resonance imaging (MRI) is one of the most effective imaging techniques; it provides a high spatial resolution and offers anatomical and functional information without using ionizing radiation. However, it also has some limitations and potential drawbacks, including long scan times, limited sensitivity to certain types of tissue, and the requirement for the use of contrast agents in some studies.<sup>1,2</sup> Currently, approximately 40% of MRI studies are contrast-enhanced studies.<sup>3</sup> Gadolinium-based contrast agents (GBCAs) have been the most commonly used contrast agents in MRI studies for many years, but concerns about their potential toxicity and side effects linked with a medical condition known as nephrogenic systemic fibrosis (NSF) have led researchers to explore alternative contrast agents, such as manganese-based and iron-based contrast agents. Manganese-based contrast agents have a long history of use in preclinical and clinical studies and have a well-established safety profile. However, they have limited availability, and their use is restricted to specific applications due to their potential toxicity at high doses.<sup>4–6</sup> Iron-based contrast agents have been developed more

recently and have shown promising results in preclinical studies. They have the advantage of being biodegradable and less likely to release toxic ions into the body compared to gadolinium-based contrast agents.<sup>7</sup>

Two primary types of contrast agents are designed to enhance tissue contrast visualization in MR imaging. T1 MRI contrast agents function by shortening the spin–lattice relaxation time of adjacent protons, whereas T2 contrast agents enhance spin–spin relaxation, thereby reducing the tissue signal.<sup>8</sup> Superparamagnetic iron oxide nanoparticles (SPIONs) are widely utilized in MRI cell tracking studies due to their remarkable sensitivity. However, SPIONs are frequently employed as T2 contrast agents, resulting in dark signals on T2-weighted images that may be challenging to distinguish from other signals, such as those caused by bleeding or calcification.<sup>9–12</sup> Consequently, T1 contrast agents are generally preferred in clinical settings, as they generate brighter signals and offer superior contrast between tissue types, making them easier to interpret. A promising new category of contrast agents, known as iron complex contrast agents, is emerging as an alternative to traditional T1 contrast agents. These agents, composed of a chelating ligand that binds to an iron ion, form a stable complex that produces T1 contrast. However, the stability of iron-based contrast agents in the body's reducing environment is a significant concern, as these agents may release toxic free iron ions. Additionally, controlling the coordination chemistry of the Fe(III) center presents a challenge due to its highly polarizing nature. These factors, along with other complexities, underscore the depth and intricacy of the research in this field. Despite these challenges, researchers are actively developing iron-based contrast agents with enhanced stability and relaxivity, showing promise for future clinical applications.<sup>13,14</sup>

The iron(III)–quercetin complex, known as “IronQ”, represents a promising new MRI contrast agent developed by the Molecular Imaging and Therapy Research Unit at the Faculty of Associated Medical Sciences, Department of Radiologic Technology, Chiang Mai University in Thailand. IronQ is a unique chemical compound composed of two integral components: Fe(III) ions, commonly referred to as ferric ions, and quercetin, a naturally occurring flavonoid that is renowned for its antioxidant properties. Dietary flavonoids, including quercetin, are well known for their potent metal-chelating abilities.<sup>15</sup> A closer examination of quercetin reveals that its molecular structure contains three phenolic rings, designated as A, B, and C, each offering potential sites for metal chelation. Additionally, quercetin exists in various forms, ranging from its neutral form (H5QT) to multiple deprotonated forms (H4QT<sup>-</sup>, H3QT<sup>2-</sup>, H2QT<sup>3-</sup>, HQT<sup>4-</sup>, and QT<sup>5-</sup>), each exhibiting varying degrees of potency in chelating metal ions.<sup>16,17</sup> The ability of quercetin to form complexes with a wide range of metal ions has been extensively documented, and this complexation significantly enhances the biological activity of quercetin compared to its free form.<sup>18–21</sup> This enhancement underscores the potential of IronQ as a powerful MRI contrast agent, combining the chelating strength of quercetin with the imaging capabilities of Fe(III) ions.

Previous studies have indicated that IronQ could serve as a “theranostic” agent, possessing both therapeutic and diagnostic properties. Specifically, IronQ has been identified as a T1-weighted MRI contrast agent owing to its paramagnetic properties. It has also been found to be non-toxic and capable of accumulating in peripheral blood mononuclear cells (PBMCs), making it a potential molecular agent for cell labeling and MRI cell tracking. Furthermore, IronQ stimulates the differentiation of PBMCs into spindle-shaped cells expressing proangiogenic cell markers, which can promote endothelial-specific differentiation and increase the limited number of endothelial progenitor cells (EPCs). These properties of IronQ may be useful in the treatment of degenerative diseases.<sup>22–26</sup> While *in vitro* studies have indicated that IronQ is a potentially low-toxicity theranostic agent, it is important to recognize that the properties and toxicity of the agent may be altered *in vivo* due to the complex interactions that can take place within a living organism.<sup>27</sup> To advance the development of IronQ as an MRI contrast agent or cell labeling tool, further *in vivo* studies are required to evaluate its safety and efficacy. Thus, this study aimed to investigate the biodistribution, pharmacokinetics, and acute intravenous toxicity of IronQ in a preclinical animal model.

## Materials and Methods

### Preparation of IronQ

IronQ was synthesized as described in previous work, with slight modifications.<sup>23</sup> In brief, quercetin (0.0050 moles) was dissolved in 500 mL of methanol, and the pH was adjusted to  $12.0 \pm 0.2$  using a 50% w/v sodium hydroxide solution. The deprotonated quercetin was then mixed with a freshly prepared ferric chloride (0.0025 moles) solution in an

equivalent volume at room temperature for 6 hours. The resulting IronQ product was concentrated in its hydrated form via rotary evaporation and subsequently lyophilized into a powder.

Key characteristics of IronQ, including its electronic transition absorption spectrum, hydrodynamic size, zeta potential, and purity, were essential to confirm before conducting further experiments. Then, IronQ powder was dissolved in distilled water to prepare a stock solution with a final concentration of 2 mg/mL for *in vitro* studies and concentrations of 60 mg/mL, 120 mg/mL, and 180 mg/mL for *in vivo* studies. All solutions were sterilized using a 0.2  $\mu\text{m}$  syringe filter. The iron content of the IronQ stock solution was quantified using inductively coupled plasma–optical emission spectroscopy (ICP-OES) to ensure accurate measurements for the relaxivity experiments.

## Characterization of IronQ

The characteristics of IronQ were determined using an Agilent 8453 UV–visible spectrophotometer, with a full scan spectrum ranging from 198 to 1100 nm. The hydrodynamic size and zeta potential were measured using a Zetasizer Nano ZS (Malvern, United Kingdom). The HPLC profile of IronQ was analyzed using a Shimadzu LC-20AD Prominence Liquid Chromatograph system equipped with an SPD20A Prominence Diode Array Detector and a DGU-20A3 Prominence Degasser (Shimadzu, Japan). Wavelength scanning was conducted between 190 and 800 nm, with precise monitoring at 294 nm. A 20  $\mu\text{L}$  sample of IronQ was injected into a ZORBAX Eclipse Plus C18 analytical column (250  $\times$  4.6 mm i.d., 5  $\mu\text{m}$  particle size) paired with an Eclipse Plus C18 analytical guard column (12.5  $\times$  4.6 mm i.d., 5  $\mu\text{m}$  particle size) from Agilent Technologies (California, USA). The mobile phase consisted of 70% water containing 0.1% v/v trifluoroacetic acid (Phase A) and 30% methanol (Phase B), with a flow rate of 1 mL/min maintained for 10 minutes.

## Cytotoxicity Assay

Human fibroblast cells and macrophages derived from the human monocytic leukemia THP-1 cell line were cultured under standard conditions (37°C, 5% CO<sub>2</sub>) in their respective growth media. A total of 5,000 cells per well were seeded into 96-well plates in 100  $\mu\text{L}$  of culture medium and allowed to adhere for 24 hours. After this initial incubation, the medium was replaced with fresh media containing IronQ at final concentrations of 0, 50, 100, 125, 250, 500, 750, and 1000  $\mu\text{g/mL}$ . Following 48 hours of treatment, the medium was carefully removed, and cytotoxic effects were assessed using the MTT assay. Briefly, MTT solution was added to each well and incubated for 4 hours at 37°C. After incubation, the formazan crystals formed were dissolved in dimethyl sulfoxide (DMSO), and absorbance was measured at 560 nm using a microplate reader.

## Human Blood Collection

A total of 30 mL of whole blood was collected from healthy male volunteers (n=5) who met the following criteria: group O blood, aged 20–30 years, no known significant health problems, and not taking any medications or iron supplements.<sup>28</sup> All volunteers completed a questionnaire to verify their health statuses. Blood samples were collected in heparin tubes, and all samples were tested for their hematocrit levels, which were confirmed to be within the range of 40–50%. The study complies with the Declaration of Helsinki and received approval from the ethics committee of the Faculty of Associated Medical Sciences, Chiang Mai University, Chiang Mai, Thailand (approval number AMSEC-66EX-018). Informed consent was obtained from all participants prior to participation in the study.

## Determination of Relaxivity of IronQ in Water and Whole Blood

The phantoms of IronQ at various concentrations (50, 100, 125, 250, 500, 750, and 1000  $\mu\text{g/mL}$ ) were prepared in ultrapure water and whole blood, with a final volume of 1 mL per tube. All MR imaging was performed on a 1.5 Tesla MRI scanner (Ingenia, Philips, Amsterdam, Netherlands). The longitudinal relaxation times (T<sub>1</sub> values) were measured by imaging the groups of samples using an inversion–recovery turbo spin echo (IR-TSE) pulse sequence: TI = [50, 100, 200, 400, 600, 1000, 1250, 1500, 2000, 2500, 3000, 3500, 3800] ms, TR = 4000 ms, TE = 12 ms. By plotting the concentration of IronQ against the inverse of the relaxation times (1/T<sub>1</sub>), the relaxivity (r<sub>1</sub>) values of IronQ were determined.

## IronQ's Stability Test

The stability of IronQ was evaluated under various physiological conditions by incubating the complex at 4°C, 25°C, and 37°C for multiple time intervals (1, 3, 5, and 7 days). Structural and compositional changes in IronQ were monitored using an Agilent 8453 UV–visible spectrophotometer to detect potential degradation or alterations in its spectral properties. Furthermore, the magnetic properties of IronQ were analyzed using MRI to measure its longitudinal relaxivity ( $r_1$ ), ensuring the preservation of its MRI contrast performance over time.

## Animal Model

Thirty-two Sprague Dawley (SD) rats, aged 6–8 weeks old, were purchased from Nomura Siam International Co., Ltd. (Thailand). All animals were exposed to a 12-hour light/dark cycle in a specific pathogen-free environment and received food and water ad libitum throughout the study. The animals were allowed to acclimate for at least one week before experimentation at the Laboratory Animal Center, Chiang Mai University, Chiang Mai, Thailand. All animal experiments and protocols were approved by the animal ethics committees of the Laboratory Animal Center, Chiang Mai University, Chiang Mai, Thailand (approval number RT022-2566) and were conducted in accordance with the OECD Test Guideline.

## Acute Toxicity Study

Twenty-four Sprague Dawley (SD) rats were randomly divided into four groups ( $n=6$ ; 3 male and 3 female rats for each group): three treatment groups and one control group. The control group was administered 0.9% normal saline, and the treatment groups were administered a single dose of IronQ at a concentration of 75, 150, or 225  $\mu\text{mol Fe/kg}$  body weight (BW). The rats were anesthetized using thiopental sodium (60 mg/kg intraperitoneal (IP) injection) before the intraperitoneal administration of the test agents. The tested dose of IronQ was 5, 10, and 15 times higher than that used in clinical practice for magnetic resonance imaging (ie, 15  $\mu\text{mol/kg}$  of Fe for Endorem<sup>®</sup>, Guerbet, Paris, France).<sup>29</sup> All rats were observed over 24 h for signs of acute toxicity, including the general appearance of the eyes, skin, and fur, as well as tremors and convulsions, and their weights were recorded before and after administration.<sup>30</sup>

After 2 weeks, the animals were euthanized, and their tissue and organs were collected for histopathological analysis and the determination of iron accumulation using Prussian blue staining. Blood samples were collected from the saphenous veins before and after the 2-week administration of IronQ for hematological and biochemical analyses.

## Histopathological Analysis and Prussian Blue Staining

The major organs, including the liver, spleen, pancreas, kidney, heart, lung, brain, bone marrow, duodenum, and diaphragm muscle, were harvested and fixed in 10% neutral buffered formalin. For the histopathological analysis, the fixed organ was embedded in paraffin and cut into approximately 2- $\mu\text{m}$ -thick sections using a microtome. The histological sections were stained with hematoxylin and eosin (H&E) and were evaluated by a pathologist regarding the toxicity of IronQ.

For the Prussian blue staining, histological sections were deparaffinized in xylene, rehydrated through a graded ethanol series, and immersed in a solution of 5% potassium ferrocyanide and 5% hydrochloric acid for 45 minutes. This was followed by counterstaining with 80  $\mu\text{M}$  neutral red.

## Pharmacokinetic Study

Four male Sprague Dawley rats were intraperitoneally administered IronQ (150  $\mu\text{mol Fe/kg}$  BW). Blood samples (300  $\mu\text{L}$ ) were obtained from the tail vein before administration and post-dosing at 5, 15, 30, 60, 90, and 120 min and 24 hours, respectively. The blood was inoculated in a heparin tube and stored at  $-20^\circ\text{C}$  until analysis.

The levels of IronQ in the blood were measured using inductively coupled plasma–optical emission spectrometry (ICP–OES). A 200  $\mu\text{L}$  whole-blood sample was added to 3 mL of a mixture of nitric acid ( $\text{HNO}_3$ ) and hydrochloric acid (HCl) in a 1:1 volume ratio. Digestion was performed on a heating plate at 60°C for 2 hours until the solution became clear. After cooling to room temperature, the digested solution was diluted to a final volume of 50 mL using 2% nitric acid.<sup>31</sup>

## In vivo Biodistribution Study Using MRI

Four male Sprague Dawley rats were anesthetized using thiopental sodium (60 mg/kg intraperitoneal (IP) injection), and a tail vein catheter was inserted. IronQ at a concentration of 225  $\mu\text{mol Fe/kg BW}$  was administered intravenously through a tail vein catheter. Whole-body MRI was performed on a 1.5 T MRI scanner (Ingenia, Philips, Amsterdam, Netherlands) using an 8-channel knee coil. The T1-weighted images were taken before the administration of IronQ, and the images at 10, 20, 30, 60, and 90 mins and 24 and 48 hours after administration were obtained using a turbo spin echo T1-weighted (T1W) and T1-weighted fat-suppressed (T1FS) sequence: TR=530 ms, TE= 10 ms.

For image analysis, all images were analyzed using the Philips DICOM viewer software. Regions of interest (ROI) were drawn, and the signal intensities were measured. The contrast-to-noise ratio (CNR) was calculated using the following equation:

$$CNR = \frac{SI_{post} - SI_{pre}}{\sigma_{background}}$$

where  $SI_{post}$  is the signal intensity after the administration of IronQ,  $SI_{pre}$  is the signal intensity before administration, and  $\sigma_{background}$  is the standard deviation of the noise in the background.

## Tissue Biodistribution of IronQ

Biological samples, including liver, spleen, kidney, and heart, were collected from rats in the control group and at 24- and 48-hours post-injection of IronQ. The tissues were sectioned into small pieces and mineralized with 70% nitric acid, followed by incubation at 60°C for 4 hours to ensure complete digestion. After digestion, aliquots were diluted with deionized water to achieve a final nitric acid concentration of 2%. The iron content in the samples was quantified using inductively coupled plasma–optical emission spectrometry (ICP-OES).

## Statistical Analysis

Pharmacokinetic parameters were calculated using a non-compartmental analysis method. The results were expressed as the mean  $\pm$  standard deviation (SD) for the groups. Statistical differences among the experimental groups were tested using either one-way ANOVA or non-parametric tests, as appropriate, using the OriginPro2023 software. Data were considered significant when a p-value of less than 0.05 was observed.

## Results

### Synthesis and Characterization of IronQ

In this study, IronQ was synthesized using a previously established method with slight modifications to optimize yield and stability. Following synthesis, the characteristics of IronQ were thoroughly analyzed. The UV-Vis spectrum exhibited a pattern consistent with prior findings, displaying characteristic absorption peaks at 294 nm and 450–700 nm, confirming the successful formation of the iron(III)-quercetin complex. The hydrodynamic size of IronQ was determined to be  $195.1 \pm 29.61$  nm, and the zeta potential was measured at  $-19.17 \pm 2.68$  mV ([Supplementary Figure S1](#)), indicating colloidal stability with minor variations compared to previous reports. To ensure structural integrity and confirm complexation, IronQ underwent further characterization using high-performance liquid chromatography (HPLC). This analysis verified the HPLC retention profile and confirmed the purity of the complex. The IronQ profile exhibits three peaks, with the main peak representing IronQ eluting at a retention time of 3.17 minutes and minor co-eluting peaks at 2.75 and 4.07 minutes, which may indicate residual in the sample ([Supplementary Figure S2](#)). These findings further support the stability and suitability of IronQ for experimental applications. The biocompatibility of IronQ was evaluated using two normal cell lines—human fibroblast cells and macrophages derived from the THP-1 cell line—prior to in vivo studies. Cell viability, assessed via the MTT assay, demonstrated excellent biocompatibility at concentrations up to 500  $\mu\text{g/mL}$  after 48 hours of treatment ([Supplementary Figure S3](#)). Minimal toxicity was observed at a concentration of 1000  $\mu\text{g/mL}$ , with cell viability ranging between 40–50%. These findings align with previous studies reporting no cytotoxicity or genotoxicity in human peripheral blood mononuclear cells (PBMCs) within the tested dose range.<sup>27</sup> Collectively, these results highlight the safety, stability, and biocompatibility of IronQ, establishing its potential as

a promising candidate for further testing in animal models. The stock solution of IronQ, with a concentration of 10 mg/mL, was determined to have a Fe content of 12.3 mM using ICP-OES. This iron content, expressed in millimolar (mM), was used to calculate the T1 relaxivity.

## Relaxivity of IronQ in Water and Whole Blood

The paramagnetic properties of IronQ were evaluated under conditions that closely mimicked the physiological environment, using ultrapure water and whole blood. This comprehensive assessment provided insights into IronQ's effectiveness as an MRI contrast agent. The T1-weighted MRI images demonstrated an apparent increase in the signal intensity as the concentration of IronQ increased. This dose-dependent image contrast enhancement was particularly pronounced in the whole blood, as illustrated in Figure 1. The enhanced contrast in the whole blood compared to ultrapure water underscores IronQ's potential for practical use in a biological setting. The longitudinal relaxation time (T1), which measures how quickly protons in water return to equilibrium after a radiofrequency pulse, consistently decreased with increasing concentrations of IronQ. This decrease indicates that IronQ effectively enhances the longitudinal T1 relaxation rate. The linear relationship between 1/T1 (the inverse of the T1 relaxation time) and the IronQ concentration, shown in Figure 2, further confirms this property. A contrast agent's longitudinal relaxivity ( $r_1$ ) is a crucial parameter that indicates its efficiency in enhancing the T1 relaxation rate per unit concentration. IronQ exhibited relaxivity of  $2.17 \text{ mM}^{-1}\text{s}^{-1}$  in ultrapure water and  $3.56 \text{ mM}^{-1}\text{s}^{-1}$  in whole blood. The higher relaxivity in whole blood suggests that IronQ is more effective in enhancing the T1 relaxation rates in a biological environment than in ultrapure water.

The study also observed slight variations in the longitudinal relaxivity of IronQ in whole-blood samples from five different volunteers, as detailed in Table 1. This variability was likely due to differences in the protein levels among individuals. Proteins in the blood can influence the interaction between IronQ and its surrounding environment, thereby

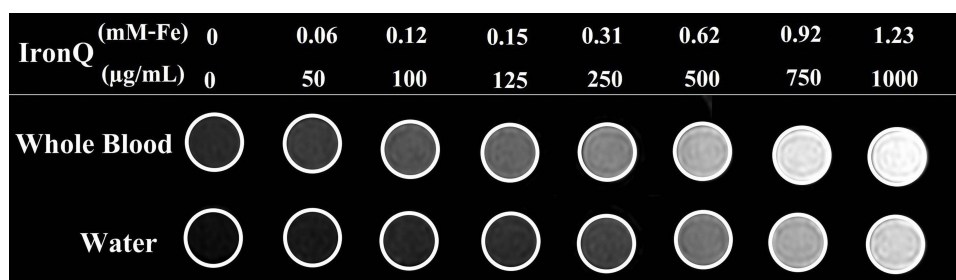


**Figure 1** T1-weighted image of phantoms containing IronQ at various concentrations.

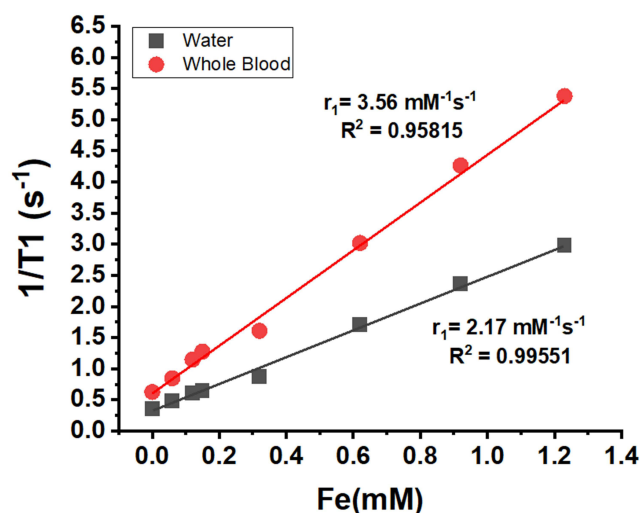


**Figure 2** The plot of 1/T1 versus the IronQ concentration in water and whole blood.

**Table 1** The Relaxivity of IronQ in Various Conditions

Condition	Water	Plasma	Whole Blood					
			Sample 1	Sample 2	Sample 3	Sample 4	Sample 5	Average
$r_1$ ( $\text{mM}^{-1} \text{s}^{-1}$ )	2.15	3.70	3.69	3.92	3.91	3.77	3.98	3.56

affecting its paramagnetic properties. Previous studies have determined the relaxivity of IronQ in plasma to be  $3.70 \text{ mM}^{-1} \text{ s}^{-1}$ ,<sup>23</sup> which is not significantly different from its relaxivity in whole blood. This similarity indicates that the presence of proteins in the blood contributes to increased relaxivity. The protein content in the blood enhances the interaction between IronQ and the surrounding environment, boosting its paramagnetic properties. The findings of this study indicate that IronQ is an effective T1 contrast agent with enhanced paramagnetic properties in physiological conditions. The dose-dependent increase in the signal intensity, the linear relationship of the T1 relaxation times and the IronQ concentration, and the higher relaxivity in whole blood all highlight the potential of IronQ for practical use in a biological setting.

Moreover, the slight variation in relaxivity among different blood samples underscores the crucial need for personalized considerations in clinical applications. The influence of the blood protein content on IronQ's performance suggests that individual patient factors, such as protein levels, should be carefully accounted for to optimize the imaging results. This emphasis on personalized considerations is vital in ensuring the effectiveness of IronQ in MR imaging.

## The Stability of IronQ

The stability of IronQ was evaluated under various storage conditions. After 7 days, the color of the IronQ solution remained unchanged, and no precipitation was observed under any of the tested conditions. However, a decrease in pH was observed after storage at  $37^\circ\text{C}$ , indicating a potential minor shift in solution acidity over extended periods, as detailed in Table 2. Despite this pH change, the UV-Vis spectrum exhibited no alterations in the characteristic absorption peaks (Supplementary Figure S4), confirming the preservation of the structural integrity of the IronQ complex. Additionally, the longitudinal relaxivity ( $r_1$ ) demonstrated slight variations, ranging from 1.9 to 2.4, as shown in Figure 3. These findings indicate that IronQ retains its stability in terms of physical appearance, molecular structure,

**Table 2** pH Value and Relaxivity of IronQ in Various Storage Conditions

Storage Condition	pH	$r_1$ ( $\text{mM}^{-1} \text{ s}^{-1}$ )
Day 1 at $4^\circ\text{C}$	$6.56 \pm 0.09$	$2.08 \pm 0.04$
Day 1 at $25^\circ\text{C}$	$6.41 \pm 0.03$	$2.36 \pm 0.05$
Day 1 at $37^\circ\text{C}$	$6.10 \pm 0.01$	$2.33 \pm 0.05$
Day 3 at $4^\circ\text{C}$	$6.50 \pm 0.08$	$1.96 \pm 0.07$
Day 3 at $25^\circ\text{C}$	$6.23 \pm 0.07$	$2.11 \pm 0.05$
Day 3 at $37^\circ\text{C}$	$5.72 \pm 0.02$	$2.12 \pm 0.05$
Day 5 at $4^\circ\text{C}$	$6.39 \pm 0.01$	$2.04 \pm 0.06$
Day 5 at $25^\circ\text{C}$	$6.09 \pm 0.05$	$2.14 \pm 0.05$
Day 5 at $37^\circ\text{C}$	$5.62 \pm 0.02$	$1.97 \pm 0.06$
Day 7 at $4^\circ\text{C}$	$6.50 \pm 0.06$	$2.17 \pm 0.06$
Day 7 at $25^\circ\text{C}$	$6.13 \pm 0.01$	$2.23 \pm 0.06$
Day 7 at $37^\circ\text{C}$	$5.38 \pm 0.02$	$2.08 \pm 0.05$

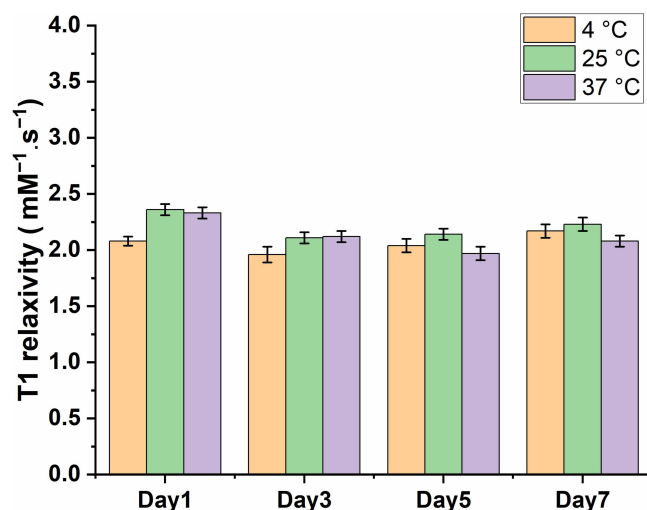


**Figure 3** The longitudinal relaxivity ( $r_1$ ) of IronQ in various storage conditions.

and relaxivity under various storage conditions. However, pH monitoring may be advisable for long-term storage, particularly at elevated temperatures, to ensure optimal performance.

### In vivo Acute Toxicity

The in vivo acute toxicity assessment of IronQ was conducted by intraperitoneally administering the compound at varying concentrations (75, 150, and 225  $\mu\text{mol Fe/kg}$ ) and monitoring the physiological responses of the test subjects over a 14-day observation period. This duration was chosen as it allowed for the detection of acute toxicity, which typically manifests within this timeframe. All rats survived this period without any significant adverse events, indicating that IronQ does not induce acute toxicity at the administered doses. The lethal dose (LD50) in the intraperitoneal administration of IronQ is more than 225  $\mu\text{mol Fe/kg}$ . Behavioral observations are crucial in detecting subtle signs of toxicity that might not be evident through other measures. In this study, no abnormal behaviors, such as lethargy or reduced mobility, were observed in the IronQ-treated groups compared to the control group. This lack of behavioral changes supports the conclusion that IronQ is well tolerated in vivo. The potential toxicity of IronQ on major organs was also evaluated, focusing on both systemic and organ-specific effects. The body weight (BW), a reliable indicator of overall systemic toxicity, was monitored throughout the study. As illustrated in Figure 4, there were no significant changes in body weight between the IronQ-treated and untreated control groups, even at varying doses, suggesting that the compound did not negatively affect the animals' overall health and metabolic status. To further assess the safety of IronQ, hematological parameters were measured, including the hemoglobin levels, white blood cell count, and platelet count. The results revealed no significant differences between the treated and control groups, indicating that IronQ does not compromise blood health. A comprehensive biochemical profile,

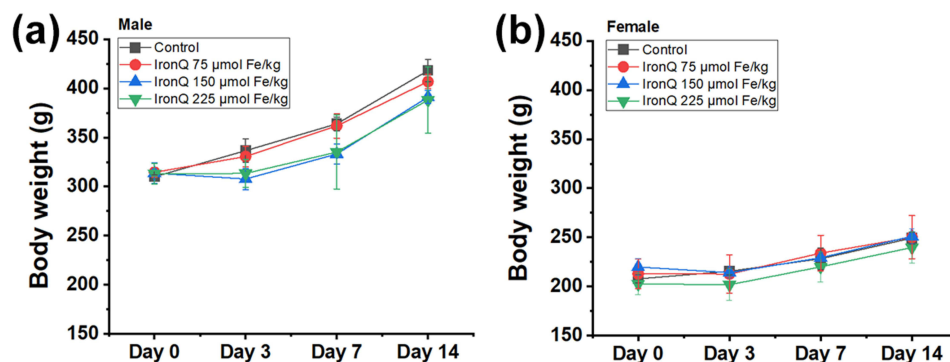


**Figure 4** Body weight curves of (a) male and (b) female Sprague Dawley (SD) rats over 14 days in the control group and the IronQ treatment groups at concentrations of 75, 150, and 225  $\mu\text{mol Fe/kg}$ .



**Table 3** Blood Analysis of Male Sprague Dawley (SD) Rats on the 14th Day Post-Treatment

Parameter	Male			
	Control	IronQ 75 $\mu\text{mol Fe/kg}$	IronQ 150 $\mu\text{mol Fe/kg}$	IronQ 225 $\mu\text{mol Fe/kg}$
<b>HEMATOLOGY PROFILE</b>				
WBC ( $\times 10^3/\mu\text{L}$ )	11.38 $\pm$ 2.51	11.06 $\pm$ 1.01	12.36 $\pm$ 5.28	9.30 $\pm$ 1.92
RBC ( $\times 10^6/\mu\text{L}$ )	7.81 $\pm$ 0.31	7.79 $\pm$ 0.35	8.93 $\pm$ 1.40	7.38 $\pm$ 0.38
HGB (g/dL)	16.00 $\pm$ 0.70	15.83 $\pm$ 0.85	17.40 $\pm$ 1.98	14.97 $\pm$ 0.15
HCT (%)	46.03 $\pm$ 2.19	46.20 $\pm$ 1.97	51.75 $\pm$ 8.13	43.77 $\pm$ 0.38
MCV (fL)	58.97 $\pm$ 0.93	59.30 $\pm$ 1.81	57.90 $\pm$ 0.01	59.40 $\pm$ 2.86
<b>BIOCHEMICAL PROFILE</b>				
Cholesterol (mg/dl)	67	69	67	65
Triglyceride (mg/dl)	242	307	196	181
HDL (mg/dl)	39	34	33	31
LDL (mg/dl)	14	14	16	14
BUN (mg/dl)	27.6	25.9	24.9	25.8
Creatinine (mg/dl)	0.56	0.53	0.48	0.52
AST (U/L)	222	147	132	167
ALT (U/L)	47	43	47	39
ALP (U/L)	278	279	258	205
Total Protein (mg/dl)	6.1	6.4	6.2	5.9
Albumin (mg/dl)	3.7	3.7	3.8	3.4

**Abbreviations:** WBC, white blood cell; RBC, red blood cell; HGB, hemoglobin; HCT, hematocrit; MCV, mean corpuscular volume; HDL, high-density lipoprotein cholesterol; LDL, low-density lipoprotein cholesterol; BUN, blood urea nitrogen; AST, aspartate transferase; ALT, alanine aminotransferase; ALP, alkaline phosphatase.

including alanine aminotransferase (ALT), aspartate aminotransferase (AST), blood urine nitrogen (BUN), and creatinine (CRE), was used to perform the liver and kidney function tests after IronQ administration. As detailed in Tables 3 and 4, there were no alterations in these biochemical markers compared with the control group. In addition, there were no significant differences between the groups treated with low-, middle-, and high-dose IronQ. These findings suggest that IronQ does not adversely affect liver or kidney function.

**Table 4** Blood Analysis of Female Sprague Dawley (SD) Rats on the 14th Day Post-Treatment

Parameter	Female			
	Control	IronQ 75 $\mu\text{mol Fe/kg}$	IronQ 150 $\mu\text{mol Fe/kg}$	IronQ 225 $\mu\text{mol Fe/kg}$
<b>HEMATOLOGY PROFILE</b>				
WBC ( $\times 10^3/\mu\text{L}$ )	6.96 $\pm$ 0.49	7.76 $\pm$ 2.06	7.32 $\pm$ 1.05	7.09 $\pm$ 0.85
RBC ( $\times 10^6/\mu\text{L}$ )	7.72 $\pm$ 0.33	7.94 $\pm$ 0.07	7.45 $\pm$ 0.41	7.99 $\pm$ 0.40
HGB (g/dL)	15.30 $\pm$ 0.60	15.70 $\pm$ 0.26	14.95 $\pm$ 0.78	15.80 $\pm$ 0.40

(Continued)

**Table 4** (Continued).

Parameter	Female			
	Control	IronQ 75 $\mu\text{mol Fe/kg}$	IronQ 150 $\mu\text{mol Fe/kg}$	IronQ 225 $\mu\text{mol Fe/kg}$
HCT (%)	44.33 $\pm$ 1.40	44.60 $\pm$ 0.70	43.15 $\pm$ 2.47	45.90 $\pm$ 1.45
MCV (fL)	57.43 $\pm$ 0.72	56.17 $\pm$ 0.47	57.95 $\pm$ 0.21	57.53 $\pm$ 1.45
<b>BIOCHEMICAL PROFILE</b>				
Cholesterol (mg/dl)	73	62	67	70
Triglyceride (mg/dl)	192	141	160	199
HDL (mg/dl)	34	37	37	30
LDL (mg/dl)	14	11	12	13
BUN (mg/dl)	31.2	25.4	28.2	28.7
Creatinine (mg/dl)	0.62	0.58	0.55	0.59
AST (U/L)	141	154	105	104
ALT (U/L)	38	36	39	38
ALP (U/L)	126	119	136	123
Total Protein (mg/dl)	6.9	6.4	6.7	6.8
Albumin (mg/dl)	4.1	4	4	4.2

**Abbreviations:** WBC, white blood cell; RBC, red blood cell; HGB, hemoglobin; HCT, hematocrit; MCV, mean corpuscular volume; HDL, high-density lipoprotein cholesterol; LDL, low-density lipoprotein cholesterol; BUN, blood urea nitrogen; AST, aspartate transferase; ALT, alanine aminotransferase; ALP, alkaline phosphatase.

The safety assessment of IronQ was performed through the histopathological examination of various organs, including the lungs, liver, kidney, bone marrow, duodenum, and spleen. This examination was performed to detect potential tissue damage, and the analysis revealed no significant signs of tissue damage or pathological changes in the IronQ-treated rats compared to the control group, as shown in Figure 5. Specifically, the lungs showed normal parenchyma with all structures intact, and no alterations were observed except for the presence of bronchus-associated lymphoid tissue (BALT), which was consistent across all groups of rats. In the liver, mild spotty necrosis was detected in some hepatocytes in the IronQ-treated rats, particularly those exposed to medium and high doses (150 and 225  $\mu\text{mol Fe/kg}$ ) of IronQ. Mild congestion was noted in the kidneys, but the lack of significant tissue damage in these organs provides reassurance about the safety of IronQ. No histopathological changes were detected in male or female rats' spleens, bone marrow, or duodena in both the IronQ-treated and control groups. The minor pathological changes observed in the liver and kidneys of the IronQ-treated rats did not significantly differ from those in the control group. These findings underscore the histopathological safety of IronQ, highlighting its non-toxic nature at both the cellular and tissue levels. To further assess the safety of IronQ, Prussian blue staining was used to detect iron accumulation in tissue. After 14 days, no iron accumulation was observed in any organ, even at the highest dose of 225  $\mu\text{mol Fe/kg}$ , as shown in Figure 6. This finding indicates that IronQ does not cause iron overload, which could lead to oxidative stress and tissue damage. The results of this acute toxicity study suggest that IronQ is well tolerated in vivo, with no significant adverse effects observed at the administered doses. The absence of changes in body weight, behavior, hematological and biochemical parameters, and histopathological integrity, and the lack of iron accumulation, support the safety profile of IronQ.

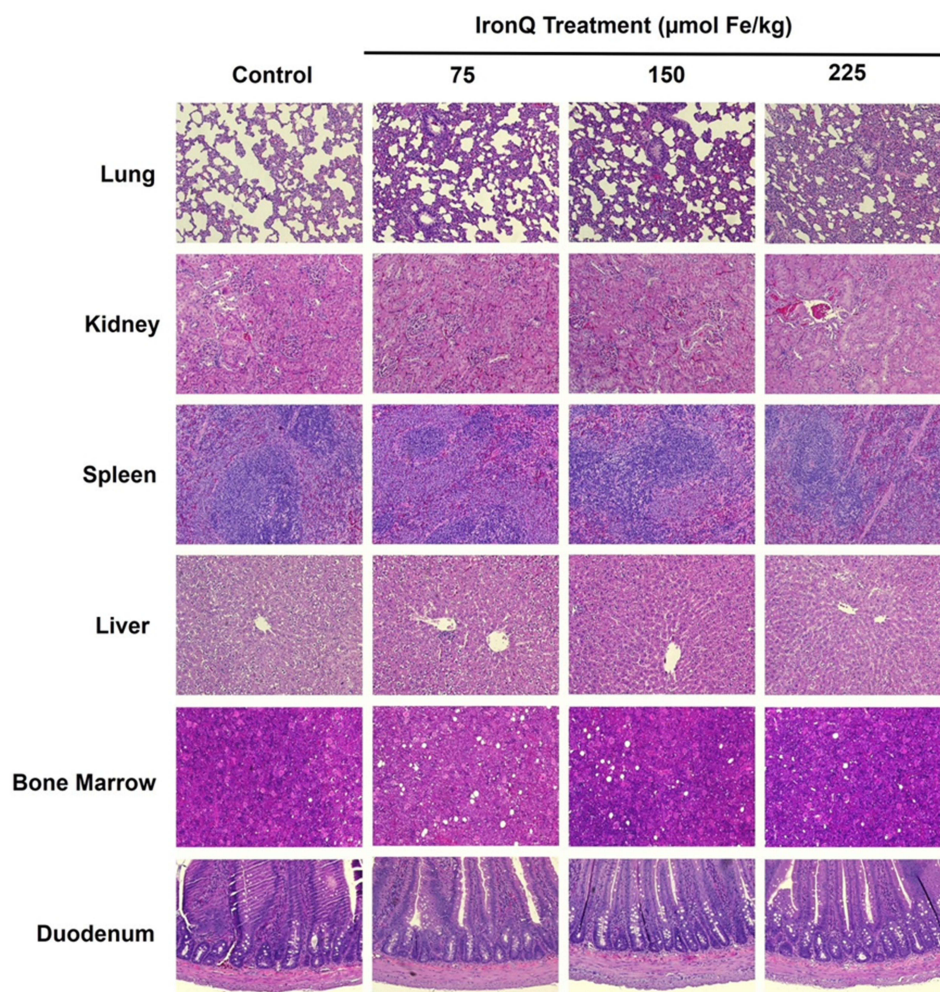


**Figure 5** Hematoxylin–eosin (H&E) staining of various tissue types, including the lungs, kidney, spleen, liver, bone marrow, and duodenum, from Sprague Dawley (SD) rats (magnification, 100 $\times$ ). Tissue samples were collected 14 days post-administration from rats treated with IronQ at a dose of 75, 150, and 225  $\mu\text{mol Fe/kg}$  and compared with those of a control group treated with normal saline solution (NSS).

## Pharmacokinetic Study

The pharmacokinetic profile of IronQ was evaluated through an experiment involving the intraperitoneal administration of 150  $\mu\text{mol Fe/kg}$  body weight to four male Sprague Dawley rats. The goal was to understand how IronQ behaves in the bloodstream over time. Blood samples were taken at various intervals up to 24 hours post-dosing to measure the iron concentrations. Inductively coupled plasma–optical emission spectrometry (ICP-OES) was utilized to precisely quantify the iron levels. The results showed a marked increase in iron bioavailability in the blood immediately following injection. The concentration–time curve (Figure 7) indicated a rapid absorption phase, with a peak plasma concentration occurring approximately  $1.1 \pm 0.72$  hours after administration. This peak plasma concentration, providing insights into the maximum level of the compound in the blood, is essential in achieving the desired diagnostic or therapeutic effect of IronQ.

The half-life ( $T_{1/2}$ ) of IronQ was determined to be around  $8.4 \pm 4.59$  hours. This measure, which indicates how long it takes for the concentration of the compound in the blood to be reduced by half, suggests a moderate elimination rate. This balanced profile ensures sufficient levels of the agent for imaging or therapeutic purposes without prolonged exposure. By 24 hours post-administration, the iron levels had returned to baseline, indicating efficient clearance from the bloodstream. This finding is crucial, as it suggests that IronQ does not remain in the body for an extended period, thereby reducing the risk of potential side effects associated with long-term exposure to iron. The rapid absorption ensures that the contrast agent quickly reaches adequate levels in the blood, making it suitable for timely imaging procedures. The moderate half-life and

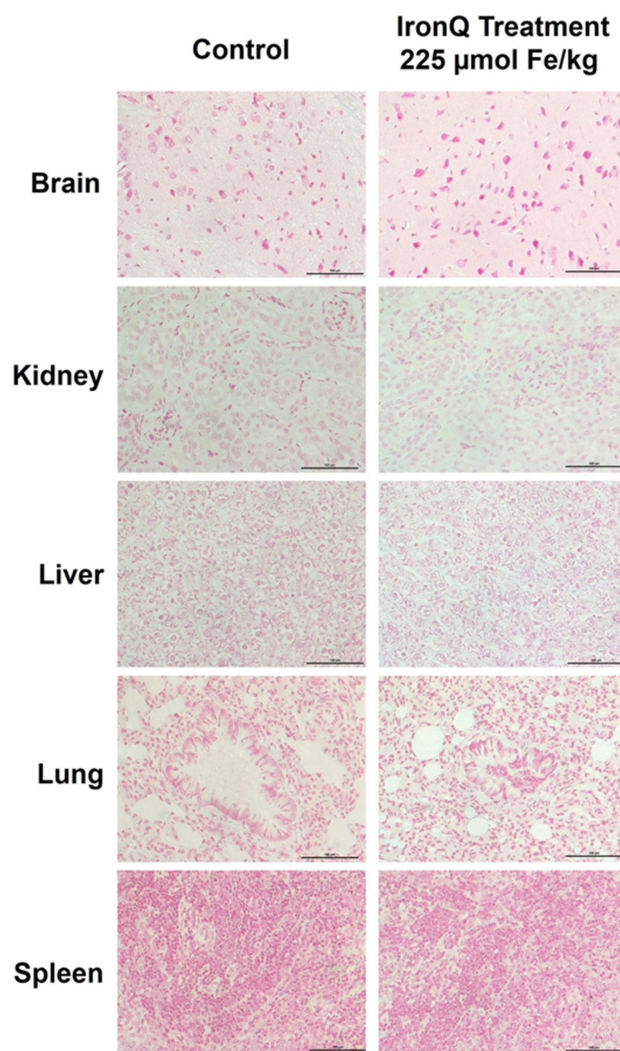


**Figure 6** Prussian blue staining of various tissue types, including the brain, kidneys, liver, lungs, and spleen, from Sprague Dawley (SD) rats (magnification, 200x). Tissue samples were collected 14 days post-administration from rats treated with IronQ at a dose of 225  $\mu\text{mol Fe/kg}$  and compared with those of a control group treated with normal saline solution (NSS).

efficient clearance reduce the risk of iron overload and related toxicity, making IronQ a safe option for repeated use if necessary. The pharmacokinetic profile of IronQ, characterized by rapid absorption, moderate elimination, and efficient clearance, underscores its potential as a practical and safe MRI contrast agent. These findings support its continued development and possible future application in clinical settings where efficacy and safety are paramount.

### In vivo Biodistribution of IronQ in Sprague Dawley Rats

The in vivo biodistribution of IronQ was evaluated using MRI and ICP-OES to determine its accumulation sites in Sprague Dawley rats. This study provides insights into the localization and clearance of IronQ following intravenous administration. After administering a single dose of IronQ at 225  $\mu\text{mol Fe/kg}$  body weight, T1-weighted MR imaging was employed to monitor its distribution. The results showed an increased signal intensity, particularly in the kidney and liver regions, with the highest signal observed at 60 minutes post-injection, as depicted in Figure 8. This indicates that IronQ rapidly accumulates in these organs. The contrast-to-noise ratio (CNR) values, detailed in Figure 9, corroborate these observations by confirming the significant increase in signal intensity in the kidneys and liver over time. This is important because the CNR is a key measure of the image quality in MRI, reflecting the degree of contrast enhancement relative to the background noise. Notably, we observed a gradual decrease in CNR values after 90 minutes, reaching

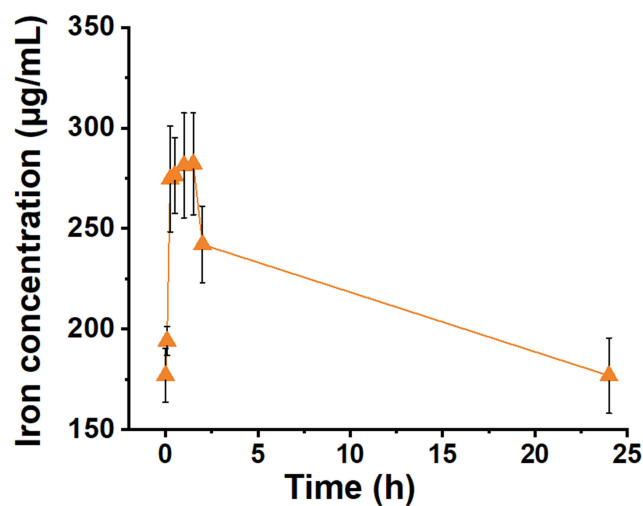


**Figure 7** The concentration-time curve of iron(III) in whole blood from Sprague Dawley (SD) rats following the intraperitoneal (IP) administration of IronQ at a dose of 150 µmol Fe/kg.

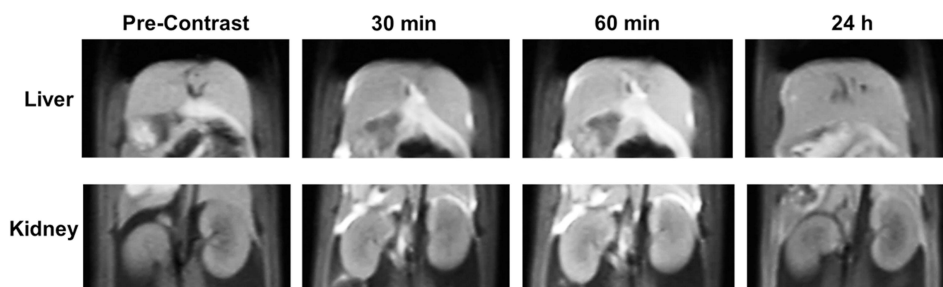


**Figure 8** Coronal T1-weighted fat-suppressed MRI images of the liver and kidneys in Sprague Dawley (SD) rats, taken before and at 30 minutes, 60 minutes, and 24 hours following the intravenous (IV) administration of IronQ at a dose of 225 µmol Fe/kg.

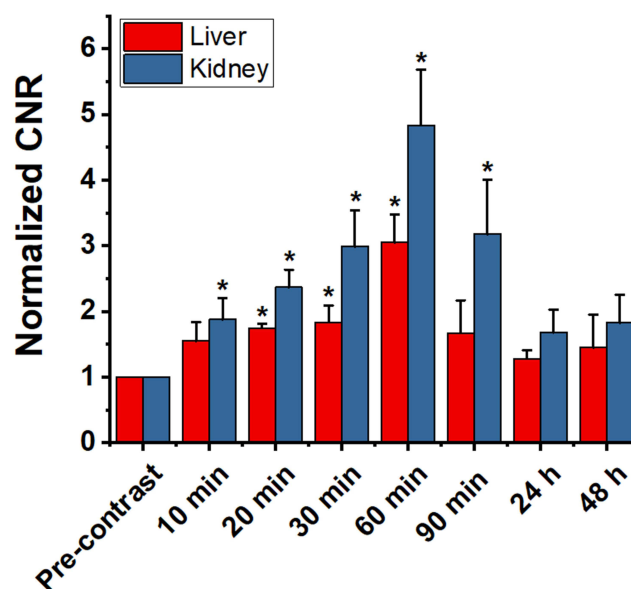


**Figure 9** Contrast-to-noise ratios (CNRs) of the liver and kidneys in Sprague Dawley (SD) rats, measured before and at various times after the intravenous (IV) administration of IronQ at a dose of 225 µmol Fe/kg. An asterisk (\*) denotes statistical significance with  $P \leq 0.05$ , highlighting time points where the contrast enhancement significantly differs from the pre-contrast image.

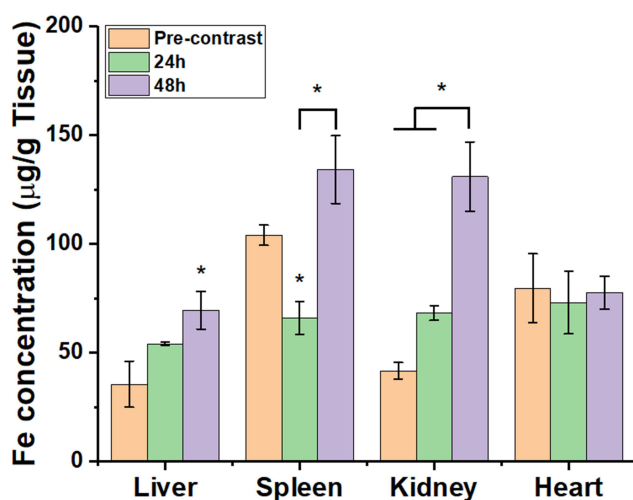


**Figure 10** ICP-OES analysis of iron content in various tissues comparing control, 24-hour, and 48-hour post-IronQ administration ( $n = 3$ ). An asterisk (\*) indicates statistical significance at  $P \leq 0.05$ .

levels similar to the baseline within 24 to 48 hours. This suggests that IronQ is subsequently cleared from the organs during this timeframe. To further confirm these findings, tissue-ICP analysis was performed at 24- and 48-hours post-injection to quantify the Fe content per gram of tissue (kidney, liver, spleen, and heart), as depicted in Figure 10. The analysis revealed an increase in Fe content in the liver and kidney, aligning with the T1-weighted MR imaging results, which demonstrated the uptake of IronQ in the kidney and liver regions. This finding is consistent with the pharmacokinetic experiment's results, which showed that the iron levels returned to baseline within 24 hours post-administration. This rapid clearance is crucial in minimizing the potential toxicity and side effects associated with the prolonged retention of the contrast agent in the body. Although IronQ demonstrated promising trends in terms of contrast enhancement, the changes were not clearly noticeable in the images. This indicates a pressing need for the further optimization of the dosing and imaging protocols to achieve clearer and more consistent contrast enhancement.

## Discussion

This study introduces the iron–quercetin complex (IronQ) as a novel theranostic agent composed of one Fe(III) ion and two quercetin molecules. Iron was chosen as the coordination metal due to its well-established efficacy as an MRI contrast agent. Iron, being an endogenous substance, offers a safer alternative to gadolinium-based agents, thereby reducing toxicity and long-term safety concerns.<sup>7</sup> Quercetin was selected as the ligand due to its extensive biological activity and multiple binding sites.<sup>31–33</sup> This unique combination enhances IronQ's potential as a theranostic agent. IronQ demonstrates significant promise as a T<sub>1</sub>-positive MRI contrast agent. Its nanoparticles are spherical in shape, water-soluble, and have a median size ranging from 100 to 200 nm. Additionally, the negative surface charge further supports its stability in biological environments.<sup>23</sup> IronQ can be efficiently internalized by various cell types through simple incubation, making it ideal for monitoring via T1-weighted MRI techniques.<sup>22–24</sup> Beyond its role in cell tracking, IronQ has shown potential as a therapeutic agent. Our recent studies demonstrated that mesenchymal stem cells (MSCs) labeled with IronQ significantly reduced the inflammation induced by an intracerebral hemorrhage (ICH) in a mouse model, leading to improved outcomes such as reduced neurological deficits, brain edema, and inflammation.<sup>25,26</sup> These findings underscore IronQ's outstanding potential as a theranostic agent, particularly in cell-based therapy applications.

In this study, we found that IronQ exhibited relaxivity of  $2.17 \text{ mm}^{-1}\text{s}^{-1}$  in ultrapure water and  $3.56 \text{ mm}^{-1}\text{s}^{-1}$  in whole blood at 1.5T, which is slightly lower than that of several commercial gadolinium-based contrast agents, such as Gd-DOTA ( $3.9 \pm 0.2$ ), Gd-DO3A-butrol ( $4.6 \pm 0.2$ ), Gd-DTPA ( $4.3 \pm 0.4$ ), Gd-BOPTA ( $6.2 \pm 0.5$ ), Gd-DTPA-BMA ( $4.5 \pm 0.1$ ), Gd-DTPA-BMEA ( $4.4 \pm 0.2$ ), Gd-EOB-DTPA ( $7.2 \pm 0.2$ ), and Gd-HP-DO3A ( $4.4 \pm 0.6$ ).<sup>34</sup> Despite the smaller spin quantum number of Fe(III) ( $S = 5/2$ ) compared to Gd(III) ( $S = 7/2$ ), Fe(III) complex-based contrast agents offer several significant advantages. As strong Lewis acids, iron ions can form robust and stable complexes with a wide range of ligands through

coordinated covalent bonds. Additionally, the body's well-regulated systems for the transport and storage of Fe(III) ions help to mitigate the long-term toxicity risks, a crucial benefit over Gd(III) ions. Furthermore, Fe(III) complexes exhibit increased relaxivity at higher magnetic field strengths, unlike gadolinium-based agents, which typically show reduced relaxivity under similar conditions. This makes Fe(III) complexes particularly desirable for use in modern MRI systems operating at higher magnetic fields.<sup>35</sup> However, the slight variation in IronQ's relaxivity observed across different blood samples is likely due to differences in protein levels among individuals. Whole blood consists of several components, including plasma, red blood cells, white blood cells, and platelets. Plasma, which makes up approximately 55% of the whole blood, primarily comprises water but also contains essential proteins such as albumin, globulins, and fibrinogen.<sup>36</sup> These plasma proteins play a critical role in modulating the relaxivity. Studies on gadolinium-based contrast agents have found that an albumin deficiency reduces the relaxivity, while elevated IgG levels enhance the relaxivity.<sup>37,38</sup> Additionally, individual variations in the relaxivity of IronQ could be caused by the oxidation state of the iron ions within the contrast agent. This state may be affected by ascorbic acid, a known reducing agent, which can convert ferric iron (Fe(III)) to ferrous iron (Fe(II)), affecting the contrast relaxivity.<sup>39,40</sup> However, the redox potential of the Fe(III)/Fe(II) couple is a critical factor to consider. Considering the potential for iron redox cycling, this can lead to the generation of reactive oxygen species (ROS) through Fenton or Fenton-like reactions, which could induce oxidative stress and cause cellular damage. Therefore, there are also concerns regarding the safety and stability of IronQ, particularly in the context of its redox activity and the potential for ROS generation.<sup>41,42</sup> These findings underscore the significant influence of individual variations, highlighting the critical need for personalized approaches in clinical applications.

The acute toxicity experiments provide compelling evidence for the safety profile of IronQ. Throughout the 14-day observation period, the absence of mortality, morbidity, and significant changes in blood biochemistry was noted, underscoring IronQ's biocompatibility. The histopathological analysis revealed only slight changes in the lungs, livers, and kidneys of rats treated with IronQ, comparable to those observed in the control group. These were, therefore, considered spontaneous lesions rather than treatment-related effects. Importantly, no irreversible organ damage was detected, which is particularly critical for IronQ's application as a theranostic agent, where safety is paramount. Furthermore, IronQ showed no signs of iron overload or accumulation in the organs during the 14-day period, reinforcing its favorable safety profile. These findings are consistent with the plasma pharmacokinetics study, which indicated that IronQ reaches peak blood iron levels approximately 1.1 hours after administration, with complete clearance within 24 hours. This relatively rapid clearance is advantageous as it minimizes the risk of prolonged exposure to free iron ions, thereby reducing the potential for toxicity.<sup>41,43</sup>

The rapid clearance of IronQ is further supported by the MRI signal enhancement data, which showed a decreasing trend in organ uptake at 24 hours post-administration. This indicates that IronQ does not persist in the body and is efficiently excreted. However, the metabolism of IronQ remains an area of ongoing investigation, as early-phase imaging has demonstrated uptake in the liver and kidneys. This suggests that IronQ may be excreted via both hepatic and renal pathways, consistent with the known influence of the particle size on biodistribution. The liver typically clears nanoparticles larger than 100 nm through the reticuloendothelial system (RES), while smaller nanoparticles (below approximately 5.5 nm) are usually filtered by the kidneys and excreted in the urine.<sup>44</sup> Given that IronQ's particles have been observed to range in size from 37 to 600 nm, it is plausible that some larger particles undergo breakdown, disassembly, or metabolism post-injection, thereby reducing their size and facilitating renal excretion. This dual clearance pathway via the liver and kidneys enhances the safety profile of IronQ by ensuring its efficient elimination from the body. Additionally, the negative zeta potential of IronQ, indicating anionic surface charges, may contribute to an extended circulation half-life by reducing protein adsorption and minimizing uptake by the RES through electrostatic repulsion with plasma proteins.<sup>45</sup> These characteristics contribute to the favorable pharmacokinetic profile of IronQ, supporting its rapid and efficient clearance, which aligns with the behavior observed in many iron-based compounds.<sup>40,41,43,46</sup>

The *in vivo* biodistribution assessment of IronQ provides valuable insights into its accumulation and clearance mechanisms, which are particularly relevant for its potential theranostic applications. The liver and kidneys, as common sites for both primary and metastatic tumors,<sup>47</sup> showed an enhanced T1 signal intensity, demonstrating IronQ's efficacy as a contrast agent and suggesting its potential utility in detecting and possibly targeting tumors in these regions. The rapid accumulation in and clearance from these organs highlight IronQ's promise as a contrast agent with a favorable safety profile, opening exciting possibilities for the future of diagnostic imaging.

However, to fully realize IronQ's clinical potential, further optimization of the dosing and imaging protocols is necessary. Future research should focus on refining these aspects to maximize the benefits of IronQ in diagnostic imaging, paving the way for its broader application in clinical settings.

## Conclusion

IronQ has significant potential in therapeutic and imaging applications due to its promising paramagnetic properties. Its T1 relaxivity value is  $3.56 \text{ mm}^{-1}\text{s}^{-1}$  in whole blood at 1.5T, making it a reliable MRI contrast agent. The acute toxicity assessments indicate that IronQ is safe at doses of up to 225 mm Fe/kg, with no adverse effects observed in the behavioral, hematological, or histopathological analyses and no iron accumulation in the major organs. The pharmacokinetic studies indicate that IronQ is rapidly absorbed, achieving a peak plasma concentration at 1.1 hours and exhibiting a half-life of 8.4 hours, which minimizes the risk of prolonged exposure. The in vivo MRI studies demonstrate contrast enhancement, particularly in the liver and kidneys, with a peak signal intensity at 60 minutes post-injection and clearance within 24 hours, suggesting efficient elimination. The size reduction process of IronQ particles, which facilitate renal elimination, requires further investigation to optimize its clinical use. These findings support IronQ's potential as a safe and effective biomedical imaging and therapeutic application agent, warranting further studies to confirm its long-term safety and efficacy.

## Acknowledgments

This work received support from the Department of Radiologic Technology, Faculty of Associated Medical Sciences, Chiang Mai University, Chiang Mai 50200, Thailand and the Faculty of Associated Medical Sciences at Chiang Mai University, Chiang Mai, Thailand (Grant Number R000028631).

## Disclosure

The authors report no conflicts of interest in this work.

## References

- Goodfellow F, Simchick GA, Mortensen LJ, Stice SL, Zhao Q. Tracking and quantification of magnetically labeled stem cells using magnetic resonance imaging. *Adv Funct Mater.* 2016;26:3899–3915. doi:10.1002/adfm.201504444
- Caspani S, Magalhães R, Araújo JP, Sousa CT. Magnetic nanomaterials as contrast agents for MRI. *Materials.* 2020;13:2586. doi:10.3390/ma13112586
- Xiao YD, Paudel R, Liu J, Ma C, Zhang ZS, Zhou SK. MRI contrast agents: classification and application (review). *Int J Mol Med.* 2016;38:1319–1326. doi:10.3892/ijmm.2016.2744
- Pan D, Schmieder AH, Wickline SA, Lanza GM. Manganese-based MRI contrast agents: past, present and future. *Tetrahedron.* 2011;67:8431–8444. doi:10.1016/j.tet.2011.07.076
- Xue X, Bo R, Qu H, et al. A nephrotoxicity-free, iron-based contrast agent for magnetic resonance imaging of tumors. *Biomaterials.* 2020;257:120234. doi:10.1016/j.biomaterials.2020.120234
- Do C, DeAgüero J, Brearley A, et al. Gadolinium-based contrast agent use, their safety, and practice evolution. *Kidney360.* 2020;1:561–568. doi:10.34067/KID.0000272019
- Asik D, Smolinski R, Abozeid SM, et al. Modulating the properties of Fe(III) macrocyclic MRI contrast agents by appending sulfonate or hydroxyl groups. *Molecules.* 2020;25:2291. doi:10.3390/molecules25102291
- Jeon M, Halbert MV, Stephen ZR, Zhang M. Iron oxide nanoparticles as T1 contrast agents for magnetic resonance imaging: fundamentals, challenges, applications, and prospectives. *Adv Mater.* 2021;33(23):e1906539. doi:10.1002/adma.201906539
- de Schellenberger A A, Kratz H, Farr TD, et al. Labeling of mesenchymal stem cells for MRI with single-cell sensitivity. *Int J Nanomed.* 2016;11:1517–1535. doi:10.2147/IJN.S101141
- Haedicke IE, Loai S, Cheng H-LM. An efficient T1 contrast agent for labeling and tracking human embryonic stem cells on MRI. *Contrast Media mol Imaging.* 2019;2019:3475786. doi:10.1155/2019/3475786
- Yun WS, Aryal S, Ahn YJ, Seo YJ, Key J. Engineered iron oxide nanoparticles to improve regenerative effects of mesenchymal stem cells. *Biomed Eng Lett.* 2020;10:259–273. doi:10.1007/s13534-020-00153-w
- Srivastava AK, Kadayakkara DK, Bar-Shir A, Gilad AA, McMahon MT, Bulte JW. Advances in using MRI probes and sensors for in vivo cell tracking as applied to regenerative medicine. *Dis Model Mech.* 2015;8:323–336.
- Botta M, Cfcg G, Tei L. High spin Fe(III)-doped nanostructures as T1 MR imaging probes. *Wiley Interdiscip Rev Nanomed Nanobiotechnol.* 2023;15:e1858.
- Palagi L, Di Gregorio E, Costanzo D, et al. Fe(deferasirox)<sub>2</sub>: an iron(III)-based magnetic resonance imaging T1 contrast agents. *J Am Chem Soc.* 2021;143:14178–14188. doi:10.1021/jacs.1c04963
- Shafabakhsh R, Asemi Z. Quercetin: a natural compound for ovarian cancer treatment. *J Ovarian Res.* 2019;12:55.
- Kasprzak MM, Erxleben A, Ochocki J. Properties and applications of flavonoid metal complexes. *RSC Adv.* 2015;5(57):45853–45877. doi:10.1039/C5RA05069C



17. Álvarez-Diduk R, Ramírez-Silva MT, Galano A, Merkoçi A. Deprotonation mechanism and acidity constants in aqueous solution of flavonols: a combined experimental and theoretical study. *J Phys Chem B*. 2013;117(41):12347–12359. doi:10.1021/jp4049617
18. Cornard JP, Merlin JC. Spectroscopic and structural study of complexes of quercetin with Al(III). *J Inorg Biochem*. 2002;92(1):19–27. doi:10.1016/S0162-0134(02)00469-5
19. Leopoldini M, Russo N, Chiodo S, Toscano M. Iron chelation by the powerful antioxidant flavonoid quercetin. *J Agric Food Chem*. 2006;54(17):6343–6351. doi:10.1021/jf060986h
20. Dehghan G, Dolatabadi JE, Jouyban A, Zeynali KA, Ahmadi SM, Kashanian S. Spectroscopic studies on the interaction of quercetin-terbium(III) complex with calf thymus DNA. *DNA Cell Biol*. 2011;30(3):195–201. doi:10.1089/dna.2010.1063
21. Ahmadi SM, Dehghan G, Hosseinpourfeizi MA, Dolatabadi JE, Kashanian S. Preparation, characterization, and DNA binding studies of water-soluble quercetin–molybdenum(VI) complex. *DNA Cell Biol*. 2011;30(7):517–523. doi:10.1089/dna.2010.1205
22. Kantapan J. Ex vivo expansion of EPCs derived from human peripheral blood mononuclear cells by iron-quercetin complex. *Biomed Res*. 2017;28:2730–2737.
23. Papan P, Kantapan J, Sangthong P, Meepowpan P, Dechsupa N. Iron (III)-Quercetin complex: synthesis, physicochemical characterization, and MRI cell tracking toward potential applications in regenerative medicine. *Contrast Media mol Imaging*. 2020;2020:8877862. doi:10.1155/2020/8877862
24. Kantapan J, Anukul N, Leetrakool N, Rolin G, Vergote J, Dechsupa N. Iron–Quercetin complex preconditioning of human peripheral blood mononuclear cells accelerates angiogenic and fibroblast migration: implications for wound healing. *Int J mol Sci*. 2021;22:8851. doi:10.3390/ijms22168851
25. Yang G, Kantapan J, Mazhar M, et al. Mesenchymal stem cells transplantation combined with IronQ attenuates ICH-induced inflammation response via Mincle/syk signaling pathway. *Stem Cell Res Ther*. 2023;14(1):131. doi:10.1186/s13287-023-03369-6
26. Yang G, Kantapan J, Mazhar M, et al. Pretreated MSCs with IronQ transplantation attenuate microglia neuroinflammation via the cGAS-STING signaling pathway. *J Inflamm Res*. 2024;17:1643–1658. doi:10.2147/JIR.S449579
27. Dechsupa N, Kosintarajit P, Kamkan K, et al. Iron(III)–quercetin complexes' safety for MRI cell tracking in cell therapy applications: cytotoxic and genotoxic assessment. *Nanomaterials*. 2022;12:2776. doi:10.3390/nano12162776
28. Carobene A, Strollo M, Jonker N, et al. Sample collections from healthy volunteers for biological variation estimates' update: a new project undertaken by the working group on biological variation established by the European Federation of clinical chemistry and laboratory medicine. *Clin Chem Lab Med*. 2016;54:1599–1608. doi:10.1515/cclm-2016-0035
29. Bellusci M, La Barbera A, Padella F, et al. Biodistribution and acute toxicity of a nanofluid containing manganese iron oxide nanoparticles produced by a mechanochemical process. *Int J Nanomed*. 2014;9:1919–1929. doi:10.2147/IJN.S56394
30. Dai Y, Wu C, Wang S, et al. Comparative study on in vivo behavior of PEGylated gadolinium oxide nanoparticles and magnevist as MRI contrast agent. *Nanomedicine*. 2018;14:547–555. doi:10.1016/j.nano.2017.12.005
31. Laur N, Kinscherf R, Pomytkin K, Kaiser L, Knes O, Deigner HP. ICP-MS trace element analysis in serum and whole blood. *PLoS One*. 2020;15(5):e0233357. doi:10.1371/journal.pone.0233357
32. Salehi B, Machin L, Monzote L, et al. Therapeutic potential of quercetin: new insights and perspectives for human health. *ACS Omega*. 2020;5:11849–11872. doi:10.1021/acsomega.0c01818
33. Deepika MPK, Maurya PK. Health benefits of quercetin in age-related diseases. *Molecules*. 2022;27:2498. doi:10.3390/molecules27082498
34. Shen Y, Goerner FL, Snyder C, et al. T1 relaxivities of gadolinium-based magnetic resonance contrast agents in human whole blood at 1.5, 3, and 7 T. *Invest Radiol*. 2015;50(5):330–338. doi:10.1097/RLI.0000000000000132
35. Thunus L, Lejeune R. Overview of transition metal and lanthanide complexes as diagnostic tools. *Coord Chem Rev*. 1999;184:125–155. doi:10.1016/S0010-8545(98)00206-9
36. Dean L. Blood groups and red cell antigens, 2005. Available from: <https://www.ncbi.nlm.nih.gov/books/NBK2263>. Accessed May 15, 2024.
37. Goetschi S, Froehlich JM, Chuck NC, et al. The protein and contrast agent–specific influence of pathological plasma-protein concentration levels on contrast-enhanced magnetic resonance imaging. *Invest Radiol*. 2014;49(9):608–619. doi:10.1097/RLI.0000000000000061
38. Yilmaz A, Ulak FS, Batun MS. Proton T1 and T2 relaxivities of serum proteins. *Magn Reson Imaging*. 2004;22(5):683–688. doi:10.1016/j.mri.2004.02.001
39. Yilmaz A, Yurdakoc M, Bernarding J, Vieth HM, Braun J, Yurt A. Paramagnetic contribution of serum iron to the spin-spin relaxation rate (1/T2) measured by MRI. *Appl Magn Reson*. 2002;22(1):11–22. doi:10.1007/BF03170519
40. Bales BC, Grimmond B, Johnson BF, et al. Fe-HBED analogs: a promising class of iron-chelate contrast agents for magnetic resonance imaging. *Contrast Media mol Imaging*. 2019;2019:8356931. doi:10.1155/2019/8356931
41. Kras EA, Snyder EM, Sokolow GE, Morrow JR. Distinct coordination chemistry of Fe(III)-based MRI probes. *Acc Chem Res*. 2022;55(10):1435–1444. doi:10.1021/acs.accounts.2c00102
42. Masson R, Roome NO. Spontaneous iron overload in Sprague-Dawley rats. *Toxicol Pathol*. 1997;25:308–316. doi:10.1177/019262339702500308
43. Jain TK, Reddy MK, Morales MA, Leslie-Pelecky DL. Biodistribution, clearance, and biocompatibility of iron oxide magnetic nanoparticles in rats. *Mol Pharm*. 2008;5(2):316–327.
44. Arami H, Khandhar A, Liggitt D, Krishnan KM. In vivo delivery, pharmacokinetics, biodistribution and toxicity of iron oxide nanoparticles. *Chem Soc Rev*. 2015;44(23):8576–8607. doi:10.1039/c5cs00541h
45. Alexis F, Pridgen E, Molnar LK, Farokhzad OC. Factors affecting the clearance and biodistribution of polymeric nanoparticles. *Mol Pharm*. 2008;5(4):505–515. doi:10.1021/mp800051m
46. Park J, Cho W, Park HJ, et al. Biodistribution of newly synthesized PHEA-based polymer-coated SPION in Sprague Dawley rats as magnetic resonance contrast agent. *Int J Nanomed*. 2013;8:4077–4089. doi:10.2147/IJN.S51684
47. Riihimäki M, Thomsen H, Sundquist K, Sundquist J, Hemminki K. Clinical landscape of cancer metastases. *Cancer Med*. 2018;7(11):5534–5542. doi:10.1002/cam4.1697

**International Journal of Nanomedicine**

**Dovepress**

Taylor & Francis Group

## **Publish your work in this journal**

The International Journal of Nanomedicine is an international, peer-reviewed journal focusing on the application of nanotechnology in diagnostics, therapeutics, and drug delivery systems throughout the biomedical field. This journal is indexed on PubMed Central, MedLine, CAS, SciSearch<sup>®</sup>, Current Contents<sup>®</sup>/Clinical Medicine, Journal Citation Reports/Science Edition, EMBase, Scopus and the Elsevier Bibliographic databases. The manuscript management system is completely online and includes a very quick and fair peer-review system, which is all easy to use. Visit <http://www.dovepress.com/testimonials.php> to read real quotes from published authors.

Submit your manuscript here: <https://www.dovepress.com/international-journal-of-nanomedicine-journal>